

Post-stack inversion of the Hussar low frequency seismic data

Patricia E. Gavotti, Don C. Lawton, Gary F. Margrave and J. Helen Isaac

ABSTRACT

The Hussar experiment was carried out in September 2011 with the purpose of acquiring low frequency seismic data to be used in inversion methods. Three wells located close to the seismic line, and a dynamite-source dataset acquired with three-component 10 Hz geophones were used for a post-stack inversion test with commercial software. Several low-frequency cut-off filters applied to the data were tested with the one from 3-5 Hz been selected as the optimum. The resultant impedance reflects lateral changes that were not present in the initial model and therefore come from the seismic reflections. Impedance changes in the target zone are not as precise as expected possibly due to limitations with seismic resolution compared to impedance logs. However, the inverted impedance shows the general trend and relative variations, which would allow monitoring changes in the reservoir as variations in the rock properties occur. A final inversion was performed to simulate traditional approaches when the low-frequency component is absent in the seismic data. Filtered seismic-data (10-15-60-85 Hz) and an initial model with a 10-15 Hz cut-off were used for this test. The results at the well locations show a good match but the lateral variation and character of the events resemble more the initial model character.

AREA OF STUDY AND INPUT DATA

The area of study is located near Hussar, central Alberta. The seismic line is 4.5 km long and passes close to 3 wells owned by Husky Energy (wells 12-27-25-21W4M, 14-27-25-21W4M and 14-35-25-21W4M), (Figure 1). Four source types were used and each source was recorded by three receiver types (reference Margrave et al 2011 for more information).

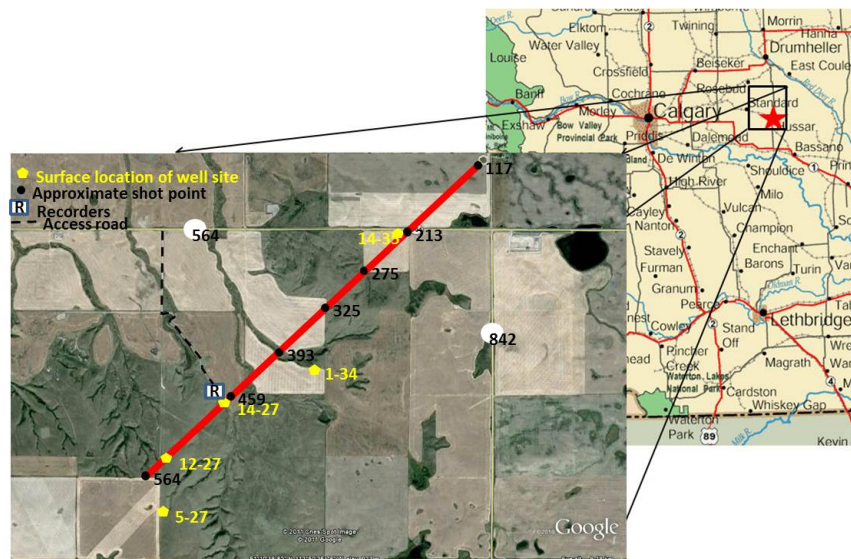


Fig. 1: Area of the study and the Hussar seismic line with the well locations nearby (modified from Margrave et al., 2011).

The data used for this paper shows the strongest low-frequency content from the following source and receiver combination: 2 kg dynamite recorded by 3C 10 Hz geophones (Margrave et al., 2011). Statics and Gabor deconvolution were applied and the data were post-stack Kirchhoff time migrated. As little processing as possible was applied so that the frequency content of the signal would not be compromised (Isaac and Margrave, 2011).

Figure 2 shows the migrated section and amplitude spectrum from the seismic line acquired using dynamite and 3C 10 Hz geophones. The locations of the three wells are also shown. Isaac and Margrave (2011) analysed and processed the dataset and showed that the dominant signal band extends from about 10 Hz to 60 Hz with an increase in power from 4 to 10 Hz.

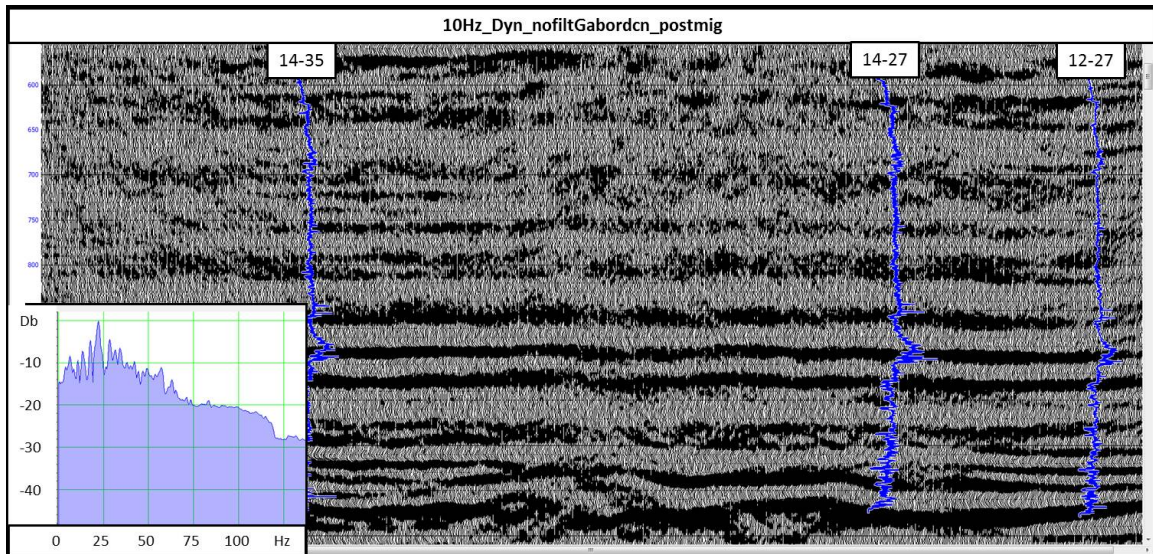


Fig. 2: 10 Hz dynamite Hussar migrated section with wells 14-35-25-21W4M, 14-27-25-21W4M and 12-27-25-21W4M. The amplitude spectrum of the unfiltered seismic data is also shown, with energy down to 4 Hz.

The vertical resolution of the seismic data is related to the minimum thickness a bed must have so that reflections from the top and bottom of the bed can be distinguished. The Rayleigh' criterion establishes that the limit of an optical instrument to distinguish separate images of objects occurs when the two diffraction images are separated by the peak-to-trough distance of the diffraction pattern (Kallweit and Wood, 1982). Widess (1973) establish the resolvability at about 1/8 of the dominant wavelength, and Sheriff (2001) defines the limit of resolution, based on the bed thickness, in 1/4 of the dominant wavelength. In this case, using an average velocity of 3400 m/s for the Glauconitic sandstone (read from the P-wave velocity log), the vertical resolution in the zone of interest can be determined as shown in Figure 3.

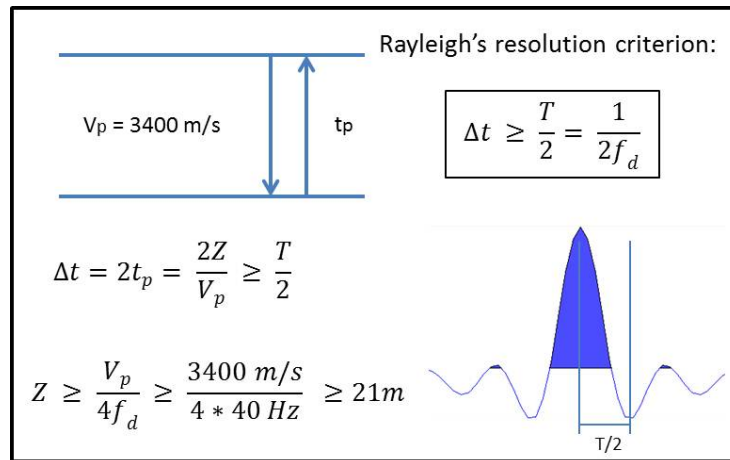


Fig. 3: Minimum bed thickness calculation based on Rayleigh's criterion where Z is the minimum thickness, V_p is the P-wave velocity, f_d is the dominant frequency, t_p is the P-wave travel time and T is the wavelength period.

The wells have good log suites including sonic and density logs. Only well 12-27-25-21W4M has an S-wave sonic log (Figure 4). Figure 5 shows the log suite of well 14-35-25-21W4M, where the Glauconitic Formation is found to be thickest (~24 m). Resistivity and porosity logs from well 14-27-25-21W4 show an increment in the target Formation (Figure 6). The porous interval is characterised by low values of gamma ray, density, P-wave velocity and P-impedance. Also, coals units are identified with lower density and impedance values.

Synthetic S-wave curves were created for wells 14-35-25-21W4M and 14-27-25-21W4 from a multi-attribute analysis with gamma ray, density and P-wave velocity curves. The S-wave from well 12-27-25-21W4M was used to train the analysis and the correlation between the predicted log and the real one resulted in 96 % (Figure 7).

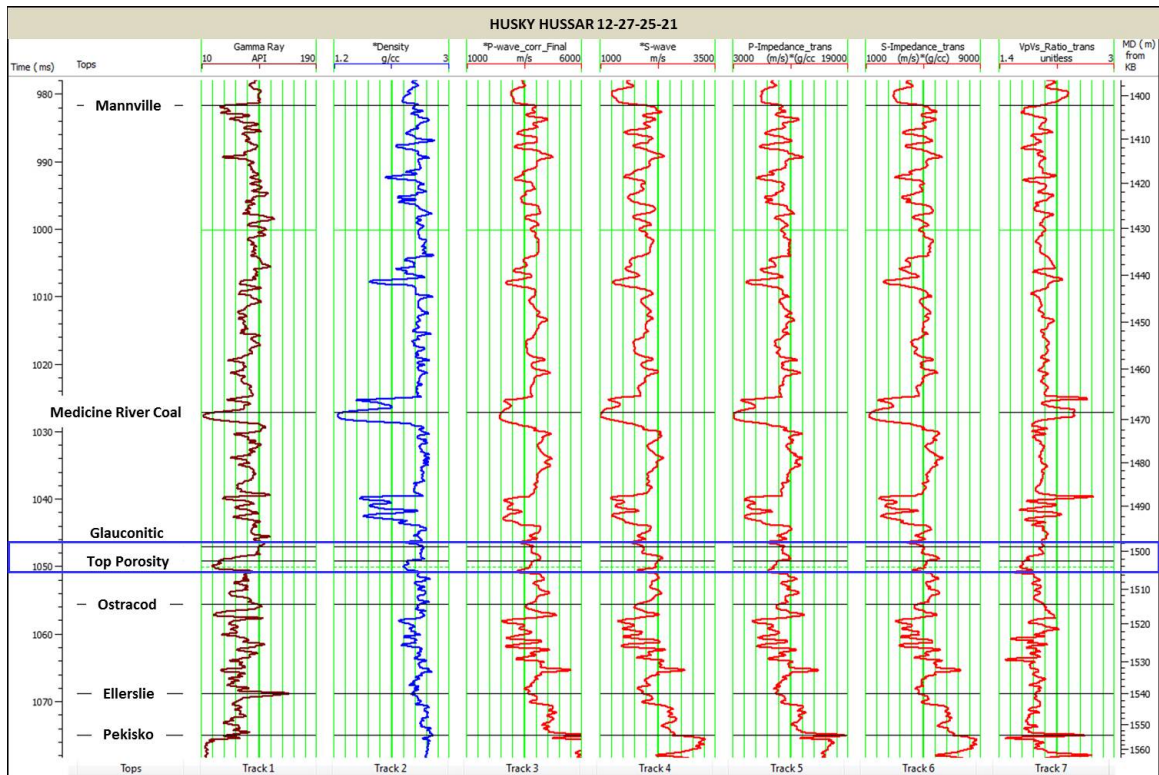


Fig. 4: Logs from well 12-27-25-21W4M. The blue rectangle highlights the Glauconitic sandstone Fm. characterised with low values of gamma ray, density, P-wave velocity, Impedance logs and Vp/Vs. Lower velocities, density and impedance values correspond to coals units within the Mannville Group.

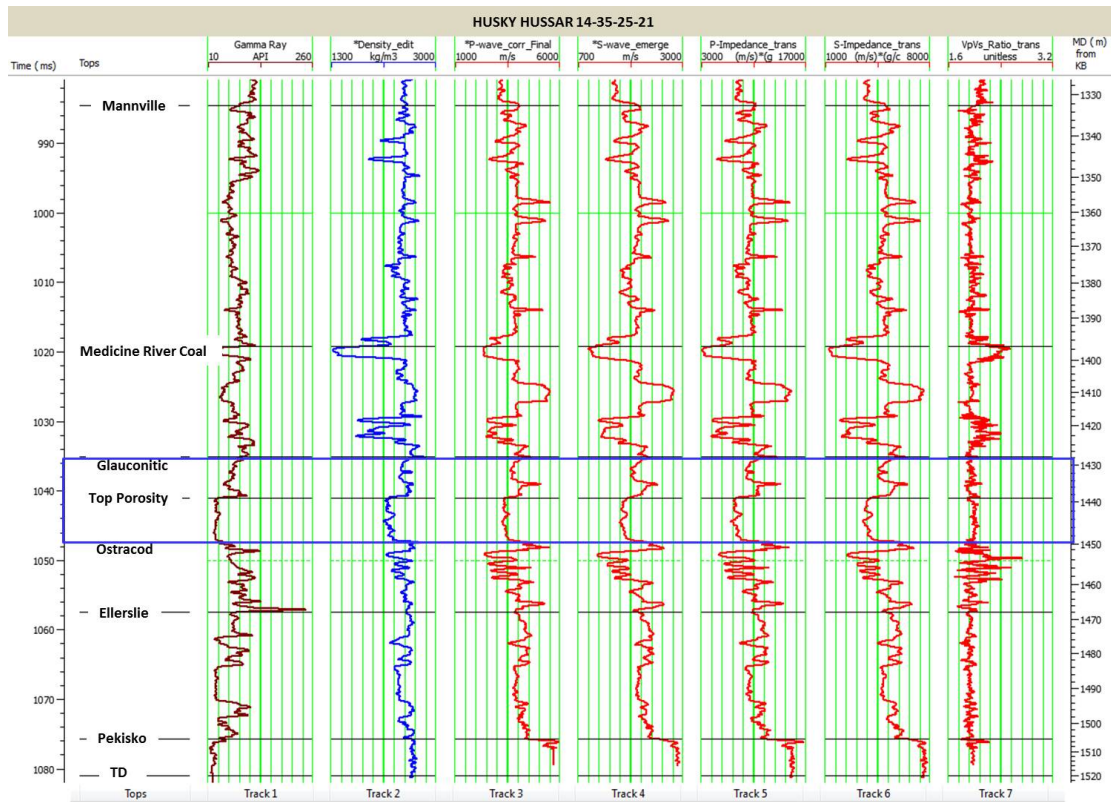


Fig. 5: Logs from well 14-35-25-21W4M. The blue rectangle highlights the Glauconitic sandstone Fm. characterised with low values of gamma ray, density, P-wave velocity and Impedance logs. Lower velocities, density and impedance values correspond to coals units within the Mannville Group.

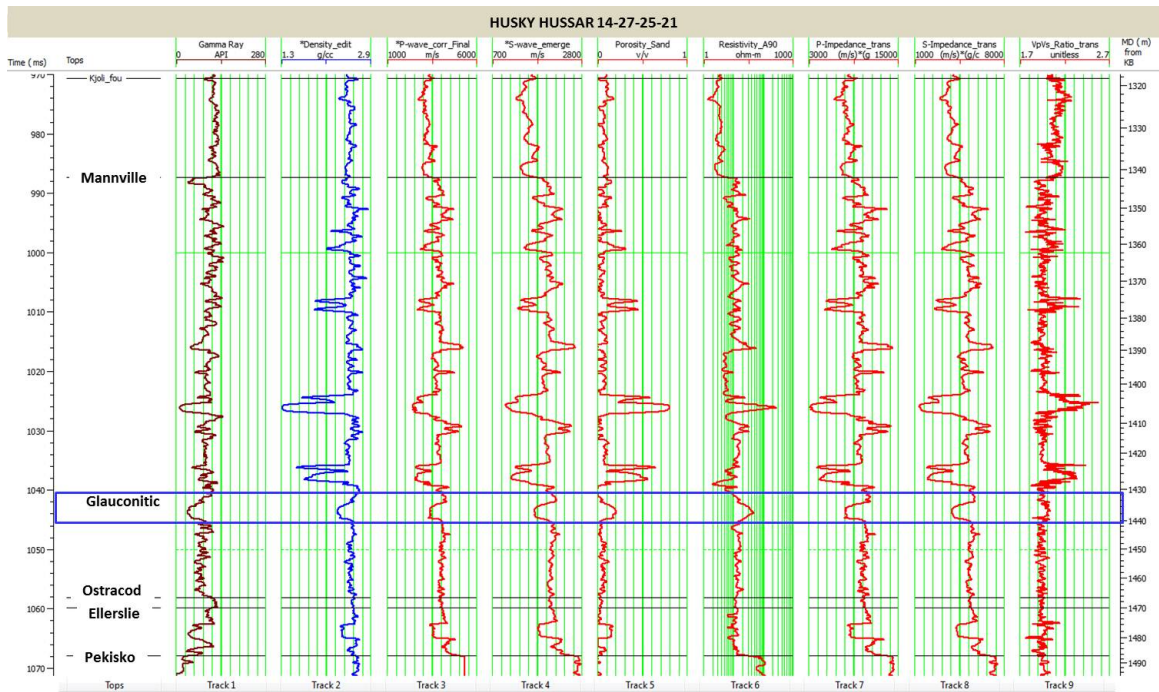


Fig. 6: Logs from well 14-27-25-21W4M. The blue rectangle highlights the Glauconitic sandstone Fm. characterised with low values of gamma ray, density, P-wave velocity and Impedance logs. Lower velocities, density and impedance values correspond to coals units within the Mannville Group.

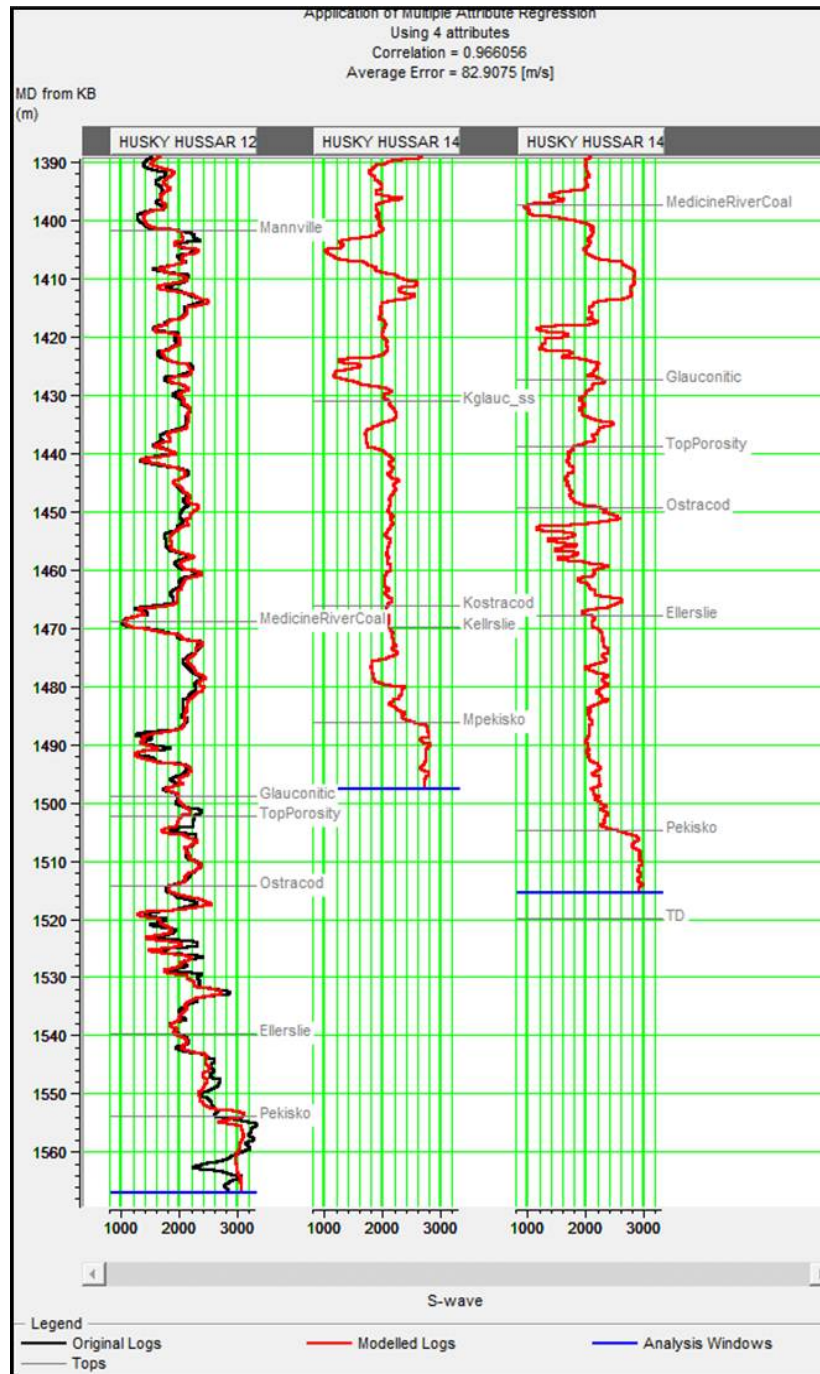


Fig. 7: Synthetic S-wave velocity curves for wells 14-35-25-21W4M and 14-27-25-21W4 from a multi-attribute analysis. The S-wave velocity log from well 12-27-25-21W4M was used to train the analysis with a correlation of 96% between the predicted log and the real one.

From a cross-plot analysis within the Mannville Group using the logs from well 12-27-25-21W4M it is possible to discriminate lithology and fluid content (Figures 8 to 11). The color key shows the gamma ray log where lower values (green < 50 API) correspond to cleaner sandstones (Figures 8 to 10). The red polygon highlights the Glauconitic Formation for high values of V_p and V_s , P-impedance values $\sim 9000 \text{ m/s} \cdot \text{g/cm}^3$ and low V_p/V_s ratio (< 1.8) possibly indicating hydrocarbon presence.

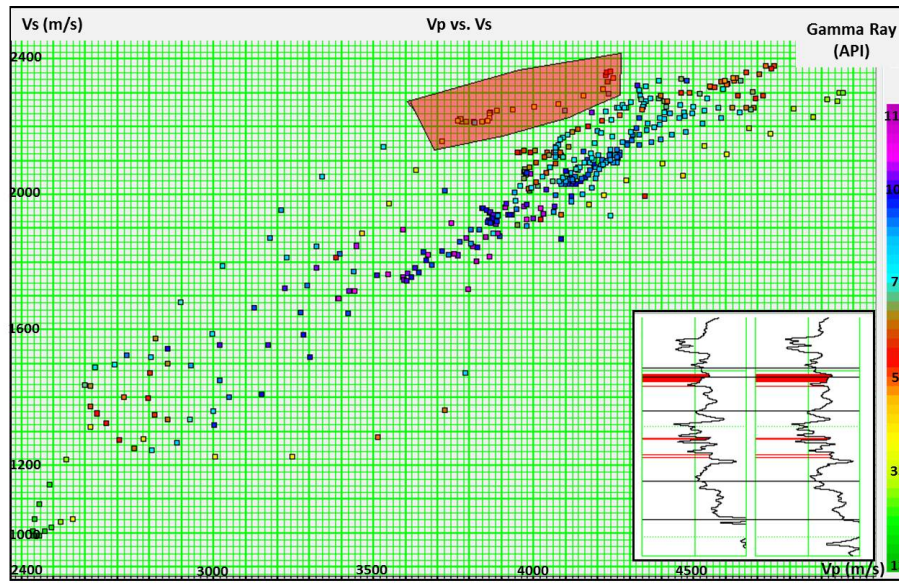


Fig. 8: Cross-plot Vp vs. Vs (Color: gamma ray) in well 12-27-25-21W4M. The red polygon highlights the Glauconitic Formation with high values for Vs and relatively high values for Vp (~3700-4300 m/s).

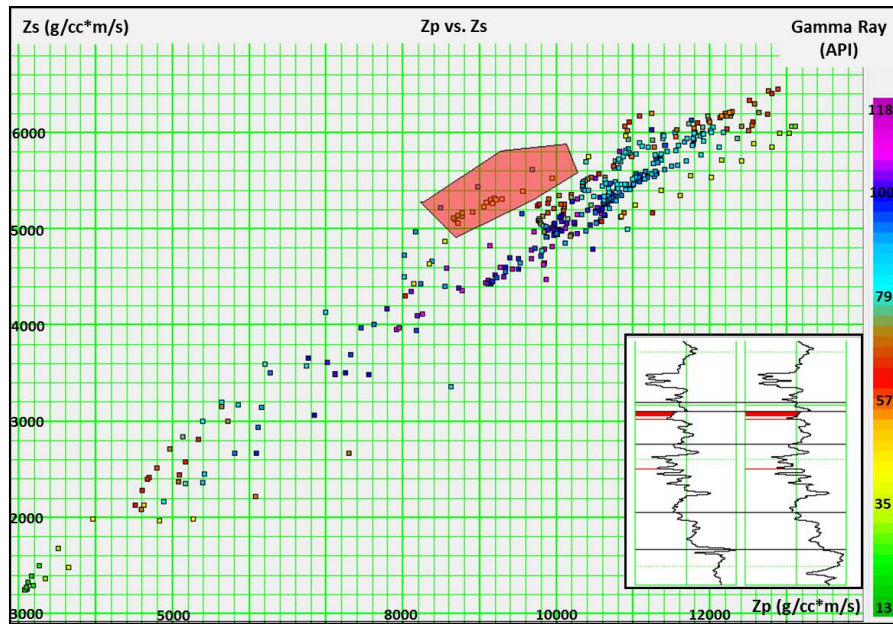


Fig. 9: Cross-plot Zp vs. Zs (Color: gamma ray) in well 12-27-25-21W4M. The red polygon highlights the Glauconitic Formation with relatively high values for both, Zp and Zs (~9000 and 5000 m/s*g/cm³ respectively).

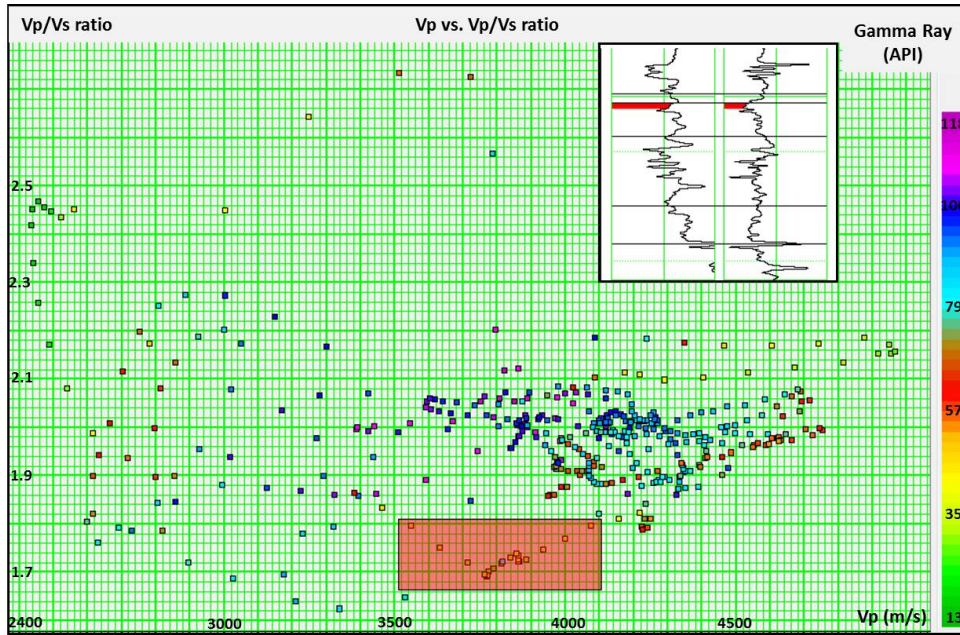


Fig. 10: Cross-plot Vp vs. Vp/Vs ratio (Color: gamma ray) in well 12-27-25-21W4M. The red polygon highlights the Glauconitic Formation with Vp values > 3500 m/s and Vp/Vs values < 1.8.

Figure 11 shows Vp/Vs vs. gamma ray with the lambda-rho property in the color bar. In this case, the isolation of the producing Formation is more evident with lower values for all these properties; this suggest that a pre-stack inversion study may be successful for discriminating lithologies and/or fluid content by the estimation of rock properties along the seismic line such as: lambda-rho, mu-rho, Vp/Vs and Vshale.

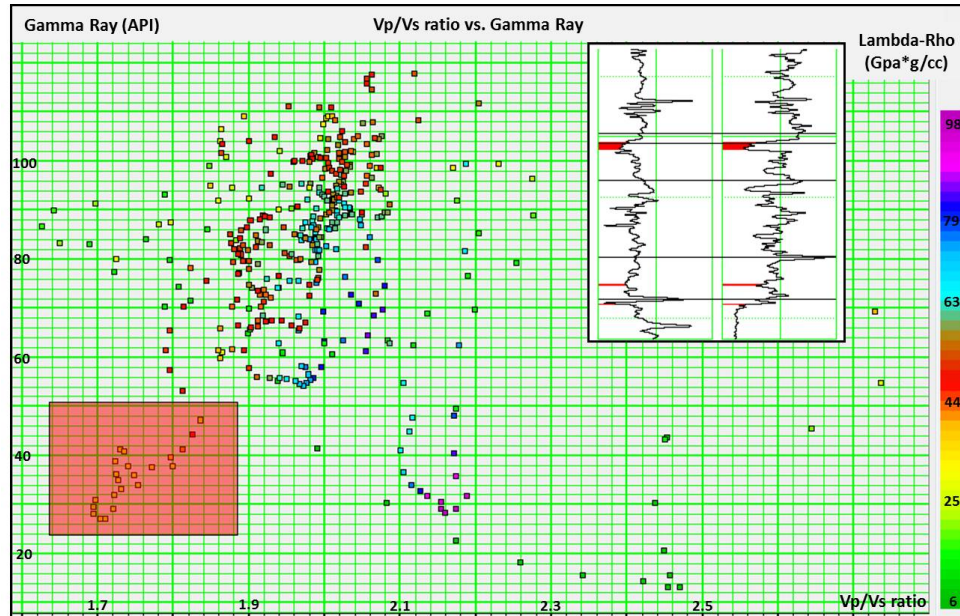


Fig. 11: Cross-plot Vp/Vs ratio vs. gamma ray (Color: lambda-rho) in well 12-27-25-21W4M. The red polygon highlights the porous Glauconitic Formation with low values for both, Vp/Vs and gamma ray.

INVERSION TEST

Inversion of seismic data is the process to produce an estimate of earth's acoustic impedance. Impedance inversion was first accomplished and reported in Lindseth (1979). Different approaches have been used for post-stack inversion, including band-limited, sparse-spike and model-based, among others (Russell and Hampson, 1991).

The way in which the Reflectivity can be extracted from the seismic is based on the convolutional model of the seismic trace according to the equation 1:

$$S = W * R + N, \quad (1)$$

where **S** is the seismic trace, **W** is the wavelet, **R** is the reflectivity and **N** is the noise and * denotes convolution. Noise is assumed to be random and uncorrelated with the signal.

Reflectivity is defined as the contrast in impedance between two interfaces (equation 2) where the impedance (**Z**) is simply the product between velocity and density:

$$R_i = \frac{Z_{i+1} - Z_i}{Z_{i+1} + Z_i}, \quad (2)$$

Band-limited impedance inversion is commonly used with the classical recursive inversion algorithm, which ignores the effect of the seismic wavelet, and treats the trace as a set of reflection coefficients (Lindseth, 1979). The inversion of seismic data is based in equation (3) from rearranging the terms of (2) to give the impedance series:

$$Z_{i+1} = Z_i \left(\frac{1+R_i}{1-R_i} \right), \quad (3)$$

The inversion requires the initial value of **Z** to be known but the limited seismic bandwidth constrains this technique. The low-frequency component missing in the seismic is added from sonic logs to assure a more realistic result (Lindseth, 1979).

The results shown here are based on the Hampson-Russell software model-based inversion approach to estimate impedance from the Hussar seismic data.

Model-based inversion

Model-based inversion (Russell and Hampson, 1991) uses a generalized linear inversion algorithm which assumes that the seismic trace (**S**) and the wavelet (**W**) are known and attempts to modify the initial model until the resulting synthetic matches the seismic trace (Cooke and Schneider, 1983).

The basic approach is to minimize this function (Hampson-Russell software. STRATA manual):

$$J = weight_1 x (S - W * r) + weight_2 x (M - H * R), \quad (4)$$

Where **S** is the seismic trace, **W** the wavelet, **R** the final reflectivity, **M** the initial guess model impedance and **H** the integration operator which convolves with the final reflectivity to produce the final impedance (* = convolution).

The initial background model is formed by blocking an impedance log from a well. The final result is dependent on the initial model so the model must be low-pass filtered to reduce this effect. Lloyd and Margrave (2011) produced a good inversion result in the well 12-27-25-21W4M location using a low cut-off of 3 Hz for the 4.5 Hz geophone receivers and found that consistent low-frequency information is present in the dynamite data as low as 1 Hz. To identify an initial model low-frequency cut-off point, several band-pass filters were applied to the seismic data to best estimate which frequency range is missing (Figure 12). Based on the amplitude spectrum and the filter tests, it is difficult to identify any coherent signal below 4 Hz, suggesting that our low-frequency cut-off can be defined around this value.

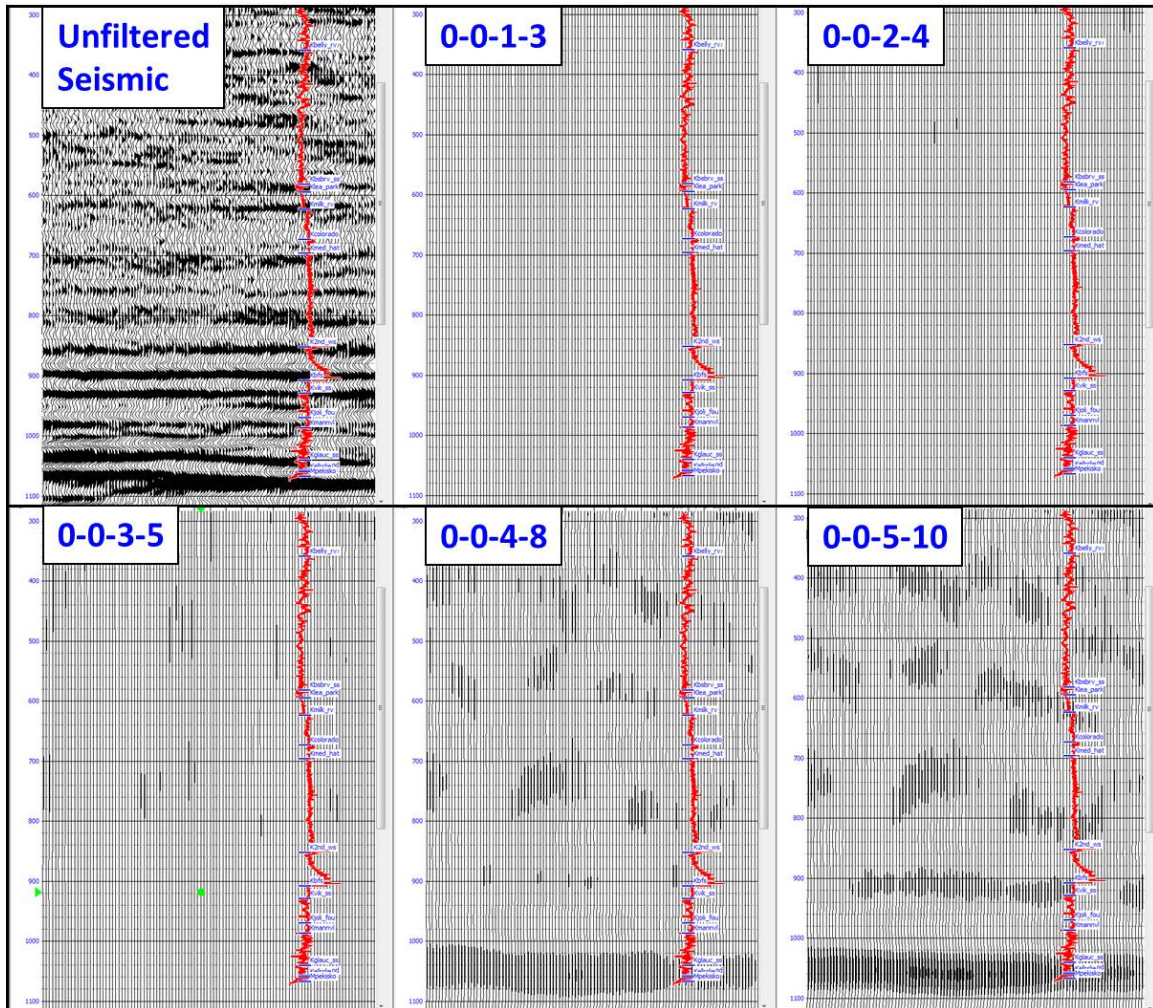


Fig. 12: Filter panels assessing low frequency data present in the seismic data. The unfiltered seismic data are displayed for reference.

Figure 13 shows an example of the impedance (Z_p) initial model generated using the P-impedance logs calculated from the sonic and density logs from well 14-35-25-21W4M and a low-pass filter of 3-5 Hz. P-impedances in the model range from 6000 to almost 12000 $\text{m/s} \cdot \text{g/cm}^3$. The 2D impedance model is generated by interpolating the impedance at the well location using the picked horizons Basal Belly River, Base Fish Scale and

Stettler Salt. The extrapolation at the top and bottom of the well curve is based on compaction trends in the well. The program uses a least squares fit to determine a trend to use for the top and bottom of the well (Dutta et al., 2009)

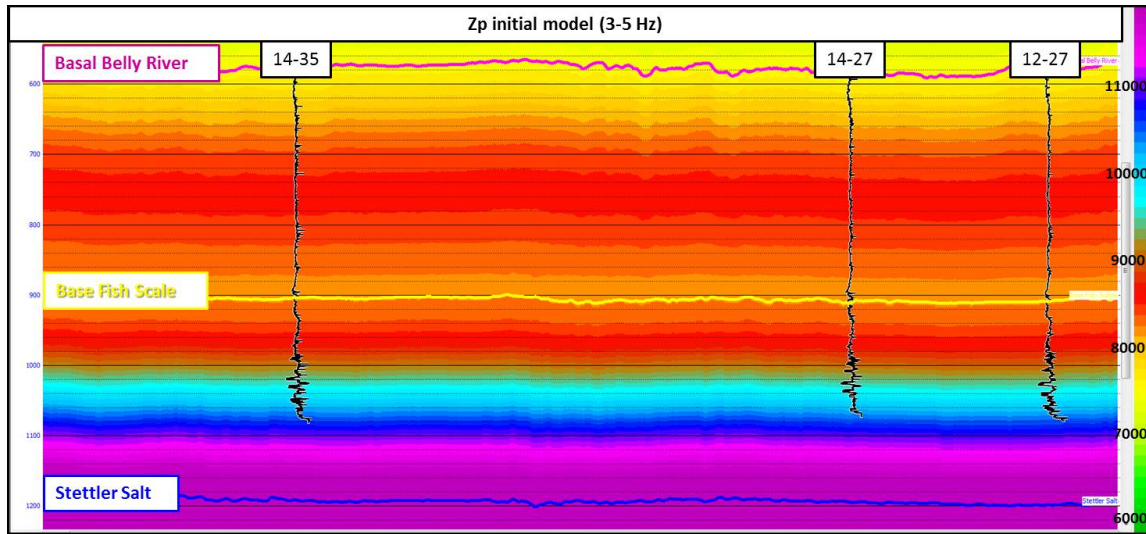


Fig. 13: Initial low frequency P-impedance model (3-5 Hz).

A post-stack inversion analysis was initially performed at the location of the well 14-35-25-21W4M, focused on a window from 500 to 1100 ms, to evaluate the accuracy of the inversion by comparing the impedance at the well with the impedance inverted from the seismic data for each of 4 initial models (1-3 Hz, 2-4 Hz, 3-5 Hz and 4-8 Hz). The impedance was inverted from a single trace at the well location and was then convolved with an extracted wavelet to produce a synthetic trace that was compared with the actual seismic trace at that location. The correlation between the synthetic (red) and the seismic trace (black) looks very good in all the cases with very high correlations coefficients (over 0.99). The estimated RMS errors were 810.769, 734.509, 729.602 and 715.934 $\text{m/s} \cdot \text{g/cm}^3$ for each model (Figure 14 and 15). As mentioned previously, the inversion result is band-limited and fails to reproduce the higher frequency details observed in the wells logs. To make a fair comparison, wells logs were filtered using a high-cut of 60/85 Hz. Within the Colorado Group the inversion estimates are very close to the actual impedance; meanwhile, within the Mannville Group the inverted impedance shows the general trend and relative variations, but several units within the Mannville Group are below the seismic vertical resolution (thicknesses $< \sim 21$ m), in which case, the amplitudes of the recorded seismic data could be affected by interference effects from surrounding layers boundaries.

To assess the inversion results elsewhere along the seismic line, a blind test was done with the wells that were not used to build the model or used in the inversion analysis. Figure 16 and 17 shows the results for well 12-27-25-21W4M and 14-27-25-21W4M respectively. The results look very similar for all the initial models. Figures 18, 19 and 20 show a cross-plot analysis between the impedance log and the inverted impedance curve for all the initial models, for each well. A small improvement in the correlation is seen when a higher limit to the low-frequency component is added with the exception of the well 14-27-25-21W4M where the correlation remains invariant at $\sim 62\%$ for all the cases.

Wells 14-35-25-21W4M and 12-72-25-21W4M show similar behaviour, the correlation is lower for the 1-3 Hz model, which is expected since there is a gap in the low-frequency component between the model and the seismic data. Since the 4-8 Hz model creates much overlap between the low frequencies from the seismic and those from the model, the 3-5 Hz model was chosen as optimum for the inversion.

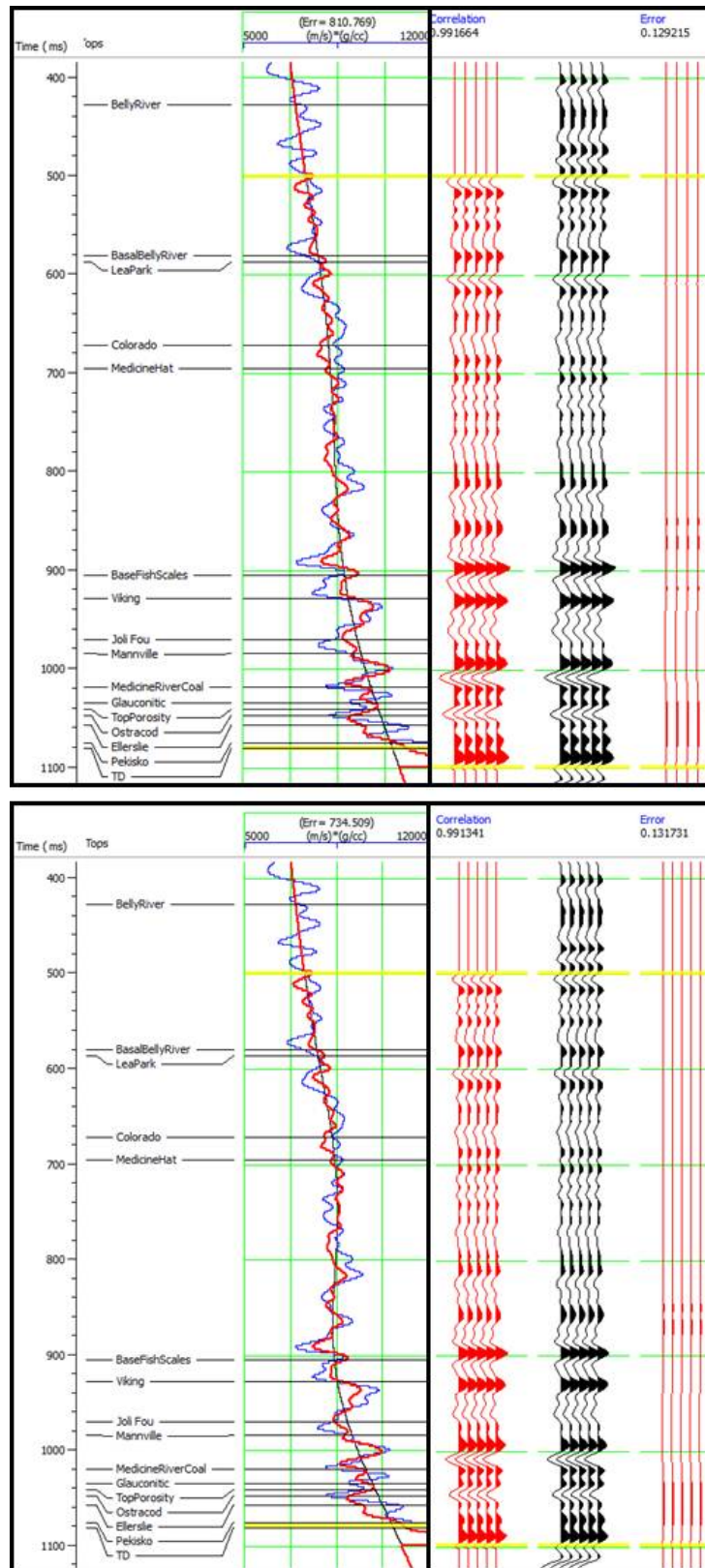


Fig. 14: Analysis of the post-stack inversion at well 14-35-25-21W4M: Impedance log (blue), initial model (black), inversion result (red), synthetic trace from inversion (red) and extracted trace from the seismic (black). Model 1-3 Hz (top) and model 2-4 Hz (bottom).

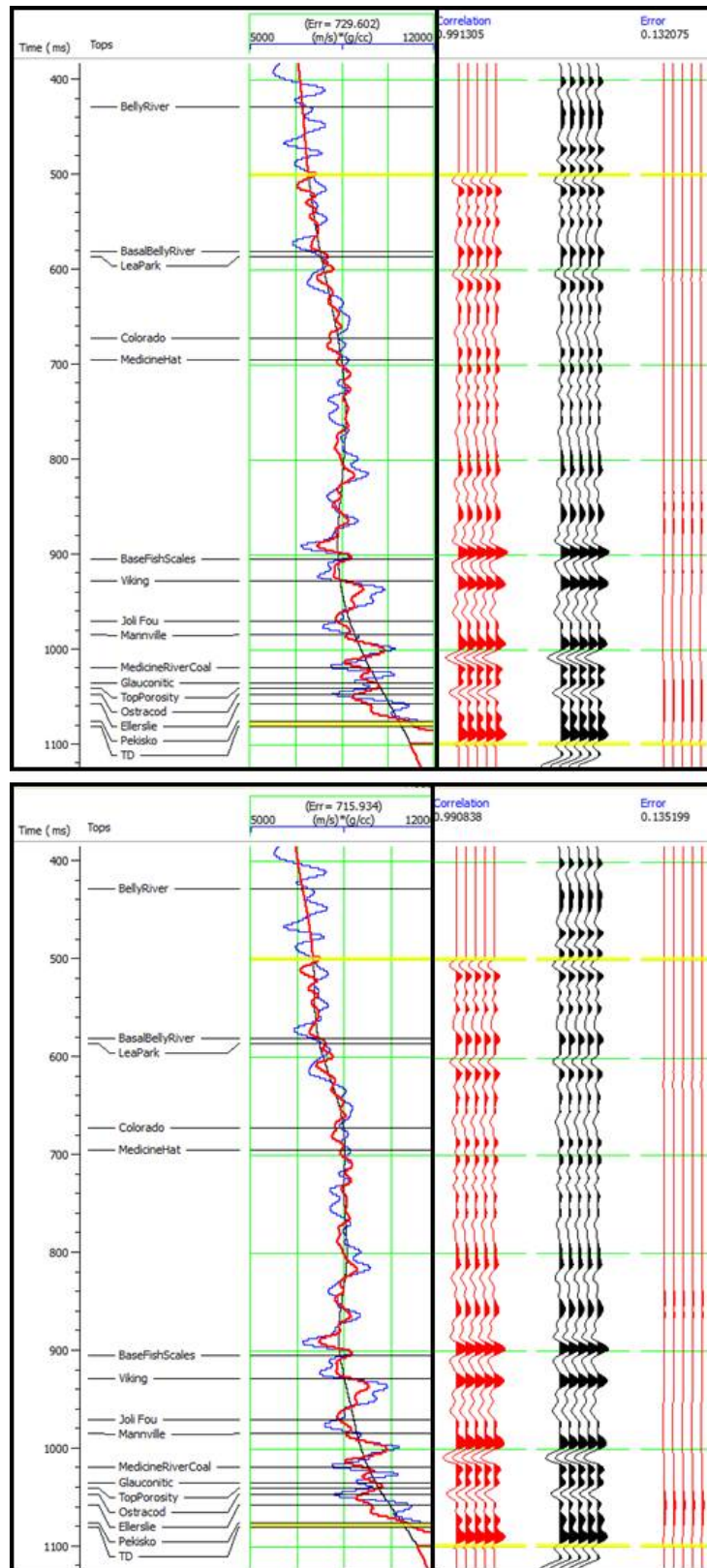


Fig. 15: Analysis of the post-stack inversion at well 14-35-25-21W4M: Impedance log (blue), initial model (black), inversion result (red), synthetic trace from inversion (red) and extracted trace from the seismic (black). Model 3-5 Hz (top) and model 4-8 Hz (bottom).

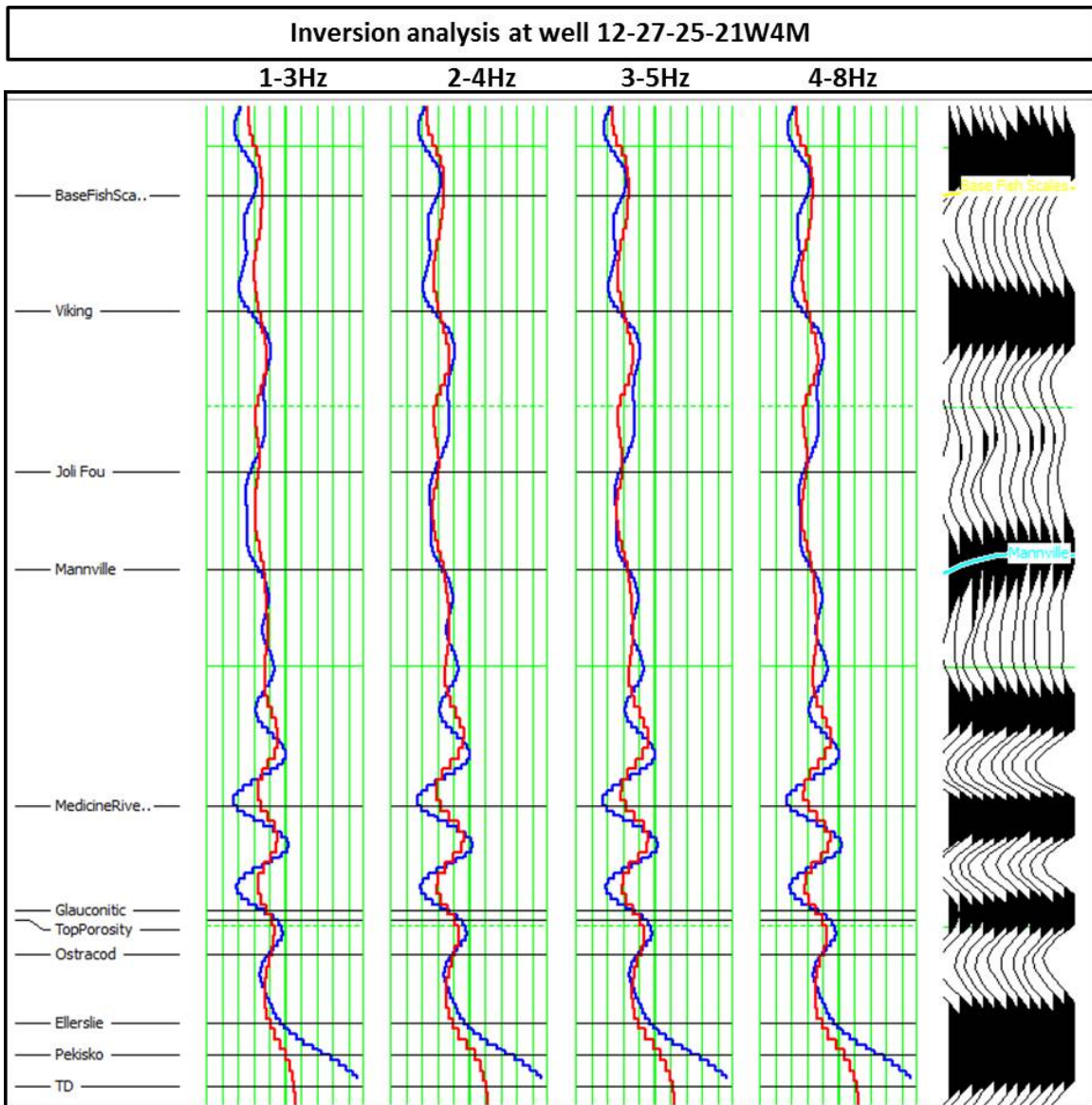


Fig. 16: Analysis of the post-stack inversion at well 12-27-25-21W4M: Impedance log (blue), inversion result (red) for each initial model.

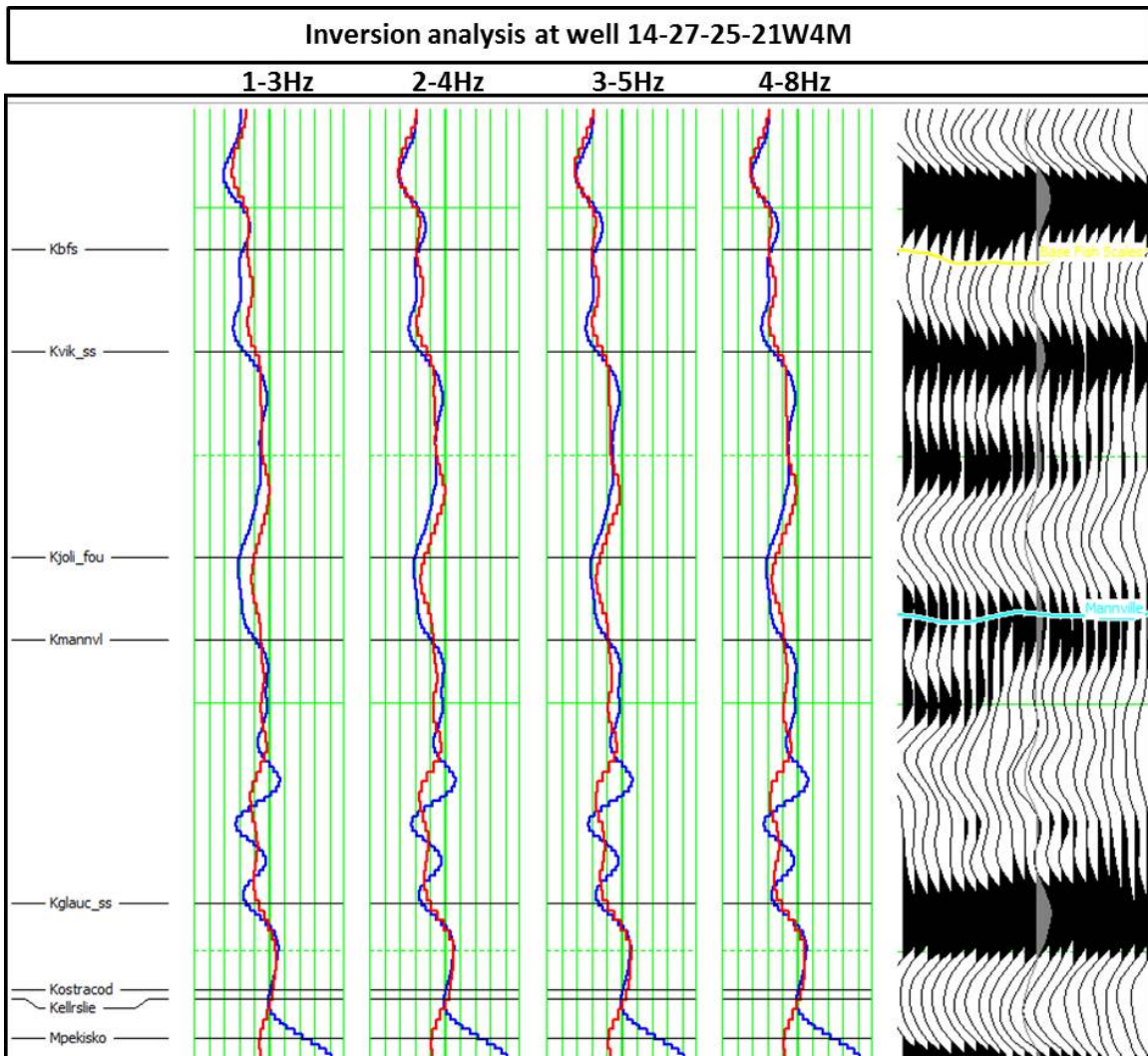


Fig. 17: Analysis of the post-stack inversion at well 14-27-25-21W4M: Impedance log (blue), inversion result (red) for each initial model.

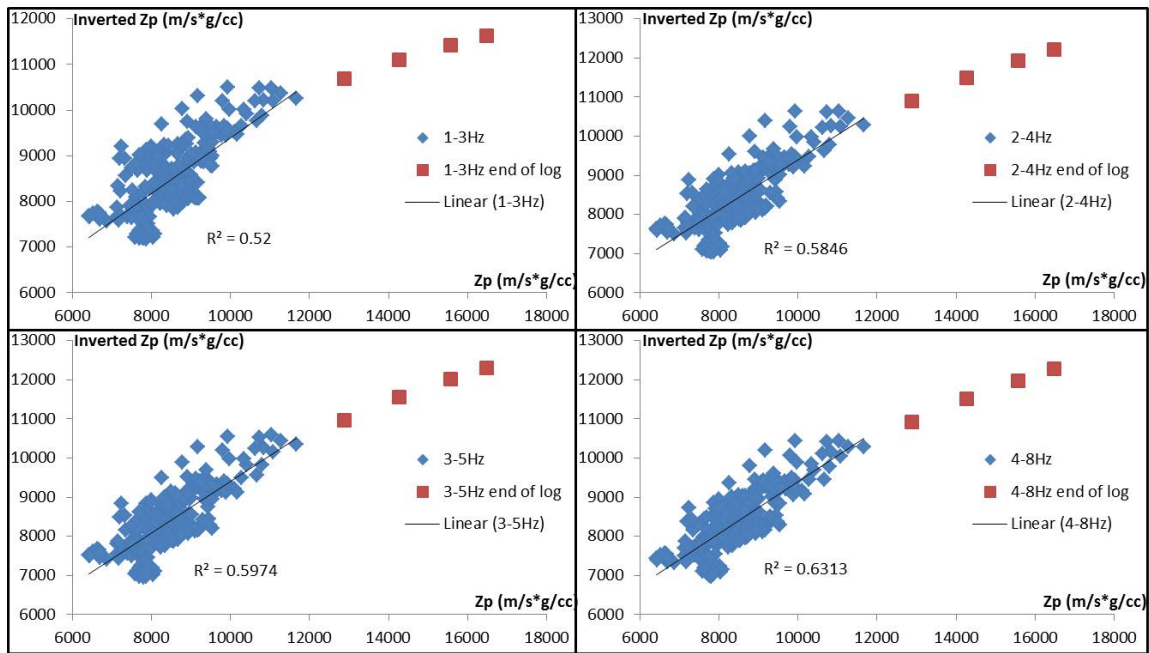


Fig. 18: Impedance log vs. Inverted impedance curve plots for well 12-27-25-21W4M for each initial model: 1-3 Hz (upper left), 2-4 Hz (upper right), 3-5 Hz (bottom left) and 4-8 Hz (bottom right). The correlation increases when a higher limit to the low-frequency component is added.

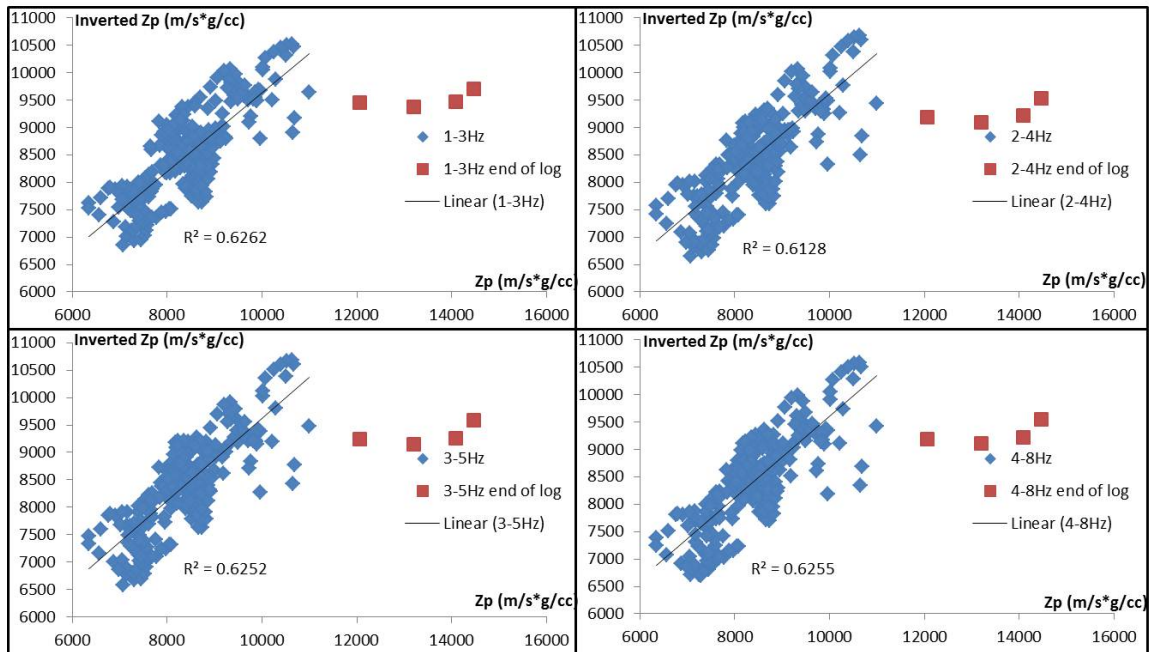


Fig. 19: Impedance log vs. Inverted impedance curve plots for well 14-27-25-21W4M for each initial model: 1-3 Hz (upper left), 2-4 Hz (upper right), 3-5 Hz (bottom left) and 4-8 Hz (bottom right). The correlation remains stable for all the cases.

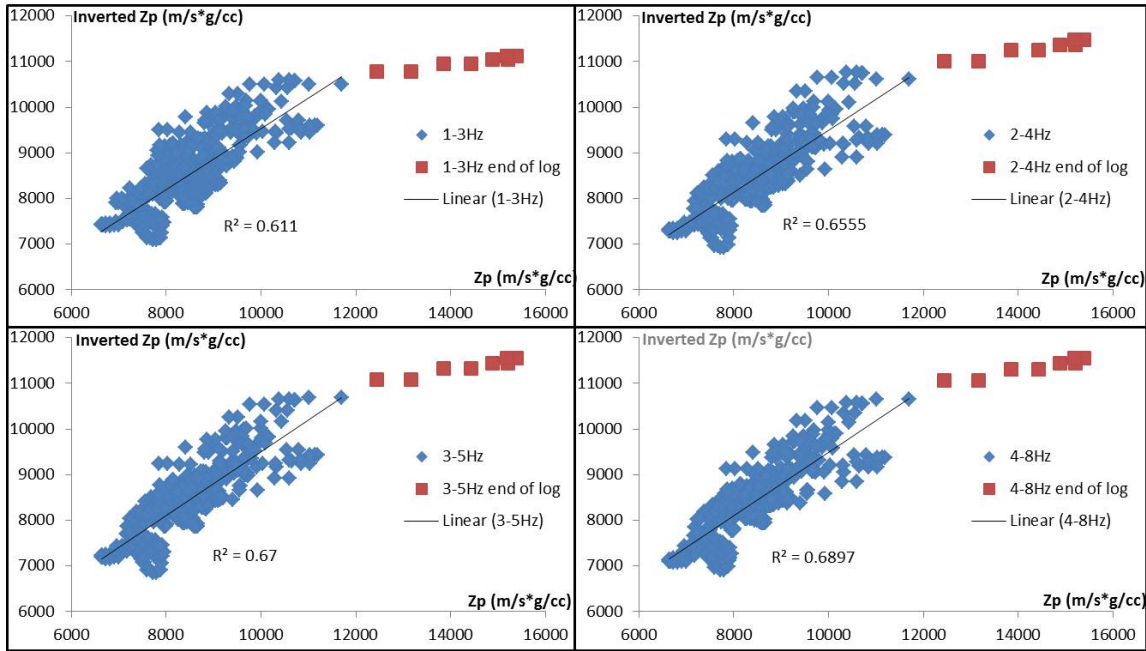


Fig. 20: Impedance log vs. Inverted impedance curve plots for well 14-35-25-21W4M for each initial model: 1-3 Hz (upper left), 2-4 Hz (upper right), 3-5 Hz (bottom left) and 4-8 Hz (bottom right). The correlation increases when a higher limit to the low-frequency component is added.

Following the analysis at the well locations, the model-based inversion of the seismic data was undertaken using the 3-5 Hz model and the multi-wells wavelet (Figure 21) resulting from the seismic-well tie process. The wavelet was extracted from well 14-27-25-21W4M and well 14-35-25-21W4M, due to the similarity in their phase and that were the wells that best tied the seismic data. The algorithm uses both the available wells and the seismic data near those wells. It extracts the wavelet by finding the operator which, when convolved with the reflectivity from the well, closely approximates the proximal seismic traces.

A single value for a hard constraint of 100% was used, indicating that the initial model can be freely modified. The inversion result (Figure 22) shows zones of low impedance (green-yellow) within the Colorado Group (Fish Scale Zone) and Upper Manville units (Glaucanitic and Medicine River Coal). Higher impedance values correspond to more shaly units (Figure 22). The P-Impedance log filtered with a high cut of 60/85 Hz was inserted for comparison with the inversion result.

The sub-units within the Manville Group are not as evident as those in the Colorado Group possibly because of resolution limitations. Most of these units have thicknesses below the seismic vertical resolution as shown previously. However, the inverted impedance shows the general trend and relative variations. The coal section is identified along the Medicine River Coal marker with values closer to the actual ones. Around 1070 ms a low impedance anomaly is seen between wells 12-27-25-21W4M and 14-27-25-21W4M which can be related to a channel within the Ellerslie Formation which is overlain by high impedance rocks possibly related to the shale unit of the Ostracod Formation.

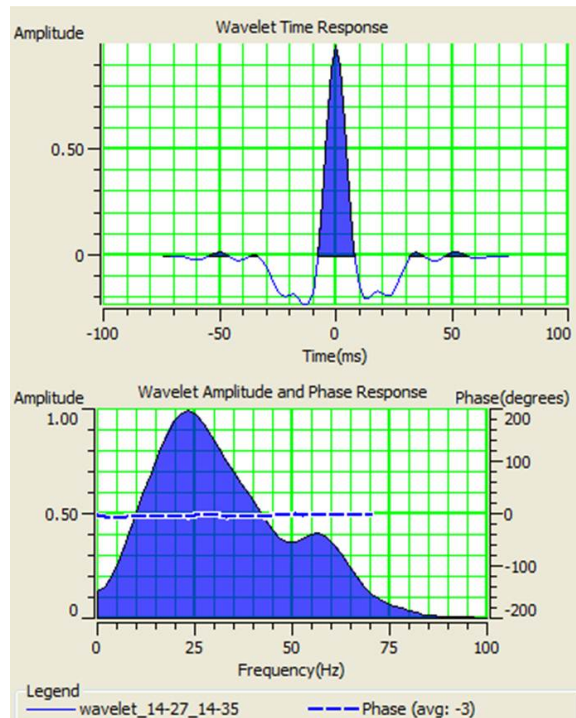


Fig. 21: Multi-wells wavelet extracted from wells 14-35-25-21W4M and 14-27-25-21W4M in a window from 500-1100 ms.

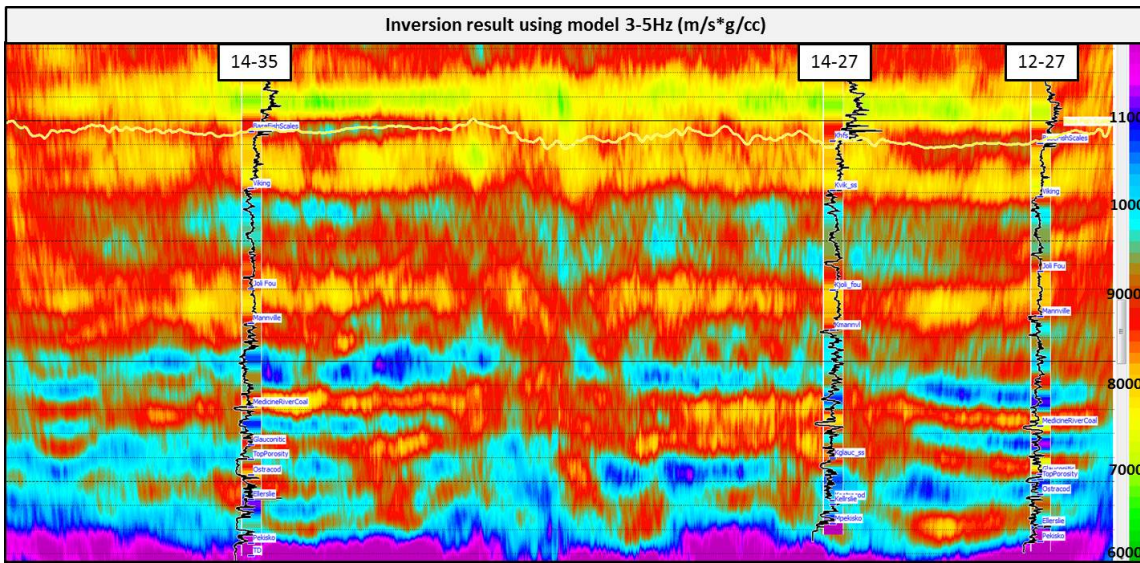


Fig. 22: Inversion result of Hussar 10 Hz dynamite dataset showing the gamma ray curve in black and the impedance log with a high-cut filter 60/85 Hz in color at the well locations for comparison.

The result shows lateral variations in the impedance of the units that was not present in the initial model. The initial model showed a general trend of increasing the impedance but without lateral variations. The changes observed in the resultant impedance reflect the

character of the seismic reflections indicating that the inversion process was dominated by the seismic data.

In comparison, a band-pass filter was applied to the input data to remove the low-frequency component recorded in the Hussar experiment, to simulate traditional cases when the low-frequency component is missing in conventional seismic data. A post-stack inversion section was generated using the same parameters except the initial model. In this case, the seismic bandwidth was 10-15-60-85 Hz and the initial model has a 10-15 Hz cut-off. Figure 23 shows the inversion result; interesting differences can be seen compared to the results shown in Figure 22. At the well locations there is a good impedance match, but the lateral variation and intensity of some events seems to be diminished and, in general, resembles more the initial model response.

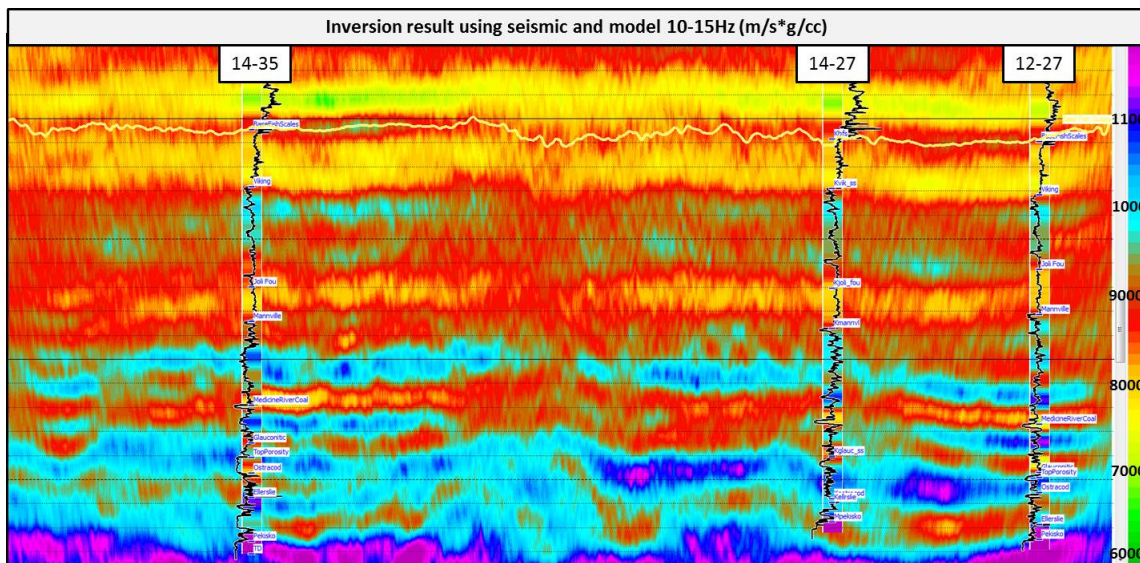


Fig. 23: Inversion result of Hussar 10 Hz dynamite dataset with a band-pass filter of 10-15-60-85 Hz showing the gamma ray curve in black and the impedance log with a high-cut filter 60/85 Hz in color at the well locations for comparison. Note the differences in continuity and character of the events with respect to the results on Figure 22.

CONCLUSIONS

A model-based post-stack inversion study was done using the low-frequency seismic data from the Hussar experiment acquired with 3C 10 Hz geophones and 2 kg of dynamite to evaluate if the inversion result improves when there is low dependence on the initial model that sometimes strongly influences the inversion result.

Four initial inversion models were tested with different low-frequency cut-offs. These all had similar results but the 3-5 Hz model was chosen to invert the seismic data since this model does not present too much overlap between the low frequencies within the seismic data with those from the model. The initial model and the inversion were undertaken with the control of the well 14-35-25-21W4M while wells 12-27-25-21W4M and 14-27-25-21W4M were used as blind tests.

The impedance determined from the inversion reflects the changes due to the seismic reflection data more than the influence of the initial model. Impedance changes in the target zone are not as detailed as was expected, possibly due to limitations with seismic resolution; however, the inverted impedance shows the general trend and relative variations which might allow monitoring changes in the reservoir to be identified when variations in the rock properties occur.

A final inversion was calculated to verify results. A band-pass filter of 10-15-60-85 Hz was applied to the seismic data to remove the low-frequency component gained during the Hussar experiment. An initial inversion model was built with a 10-15 Hz cut-off to invert this seismic data and the results at the well locations showed a good match but the lateral variation and intensity of the events were subtle and resembled more the initial model character. This is observed when the low-frequency component is missing in conventional seismic data.

ACKNOWLEDGEMENTS

We thank CREWES sponsors and members for financing and supporting this research and the Hussar experiment. We also thank Hampson-Russell for providing inversion software used in this research and Husky Energy, Geokinetics and INOVA for enabling the Hussar experiment.

REFERENCES

- Cooke, D. A. and Schneider, W.A., 1983, Generalized linear inversion of reflection seismic data: *Geophysics*, v. 48, p. 665-676.
- Dutta, T., Mavko, G., and Mukerji, T., 2009, Compaction trends for shale and clean sandstone in shallow sediments, Gulf of Mexico: *The Leading Edge*, Vol. 28, No. 5, p. 590-596.
- Hampson-Russell. (2009). Hampson-Russell Software Documentation (STRATA module). Hampson-Russell, a CGGVERITAS Company.
- Lindseth, R.O., 1979, Synthetic sonic logs – A process for stratigraphic interpretation: *Geophysics*, 44, 3-26.
- Lloyd, J. E. and Margrave, G. F., 2011, Comparison of low frequency seismic data to well logs - Hussar example: *CREWES Research Report*, Vol. 23, No. 72.
- Isaac, J. H. and Margrave, G. F., 2011, Hurrah for Hussar! Comparisons of stacked data: *CREWES Research Report*, Vol. 23, No. 55.
- Kallweit, R.S. and L.C. Wood, 1982, The limits of resolution of zero-phase wavelets: *Geophysics*, 47, 1035-1046.
- Margrave, G. F., M. B. Bertram, D. C. Lawton, K. A. H. Innanen, K. W. Hall, L. Mewhort and M. Hall, 2011, The Hussar Low-Frequency Experiment: *CREWES Research Report*, Vol. 23.
- Russell, B., and D. Hampson, 1991, Comparison of poststack inversion methods: 61st Annual International Meeting, SEG, Expanded Abstracts, 10, 876-878.
- Sheriff, R.E., 2002, *Encyclopedic Dictionary of Applied Geophysics*: SEG, 4th ed. p.429.
- Widess, M.B., 1973, How thin is a thin bed?: *Geophysics*, 38, 1176-